Magnetization and critical current of finite superconducting $YBa_2Cu_3O_7$ rings

E. Bartolomé, X. Granados, A. Palau, T. Puig, and X. Obradors
Institut de Ciència de Materials de Barcelona, CSIC, Campus U.A. Barcelona, 08193 Bellaterra, Spain

C. Navau
Escola Universitària Salesiana de Sarriá (EUSS), Ps. Sant Joan Bosco 74, 08017 Barcelona

E. Pardo and A. Sánchez
Grup d'Electromagnetisme, Departament de Física, Universitat Autonoma de Barcelona, 08193 Bellaterra, Spain

H. Claus
Material Science Division, Argonne National Laboratory, Argonne, Illinois, USA
(Received 2 August 2004; revised manuscript received 8 February 2005; published 15 July 2005)

The irreversible magnetization of finite melt-textured $YBa_2Cu_3O_7$ rings in perpendicular applied fields, affected by demagnetizing effects, is presented. The influence of the ring aspect ratio on the initial flux penetration and magnetization loops is studied by Hall probe and SQUID magnetometry. A general methodology based on the critical state model is developed in order to determine the critical current density from the field of full penetration H_{pen} in finite rings. We demonstrate that due to the field dependence of the critical current, the full penetration field H_{pen} of a finite ring does not coincide in general with the "kink" appearing in the initial magnetization curve. However, under certain conditions [very thin/narrow rings, or weak $J_c(H)$ dependence] the two fields collapse, and the critical current density can then be easily determined from the "kink" in the initial magnetization curve. In this latter situation, we develop an expression to determine the critical current density from the magnetic field measured at the center of the ring by Hall probe magnetometry.

DOI: 10.1103/PhysRevB.72.024523 PACS number(s): 74.72.Bk, 74.25.Sv, 74.25.Ha

I. INTRODUCTION

Ring-shaped $YBa_2Cu_3O_7$ (YBCO) superconductors are key components in power applications such as magnetic bearings[1,2] or inductive fault current limiters.[3–6] In addition, superconducting rings provide a suitable geometry to make very sensitive inductive measurements allowing the determination of the critical current density J_c in single-crystalline samples,[7–10] or the intergranular critical currents in polycrystalline rings.[11,12] The recent development of techniques for welding bulk melt-textured $YBa_2Cu_3O_7$ materials[13] has renewed the interest for this geometry, since the joint performance can be evaluated with a very low voltage criterion ($<10^{-12}$ V), without making electrical contacts.[14–16] However, the typical finite dimensions of these rings hinders the straightforward application of the existing expressions of the Bean critical state model[17] for infinitely long, or very thin superconducting rings.[18] Hence, the understanding of the irreversible magnetic behavior of melt-textured bulk YBCO rings in the presence of perpendicular applied fields is a prerequisite for the correct determination of the critical currents.

In finite rings, the open connected geometry of the sample together with the important demagnetizing effects occuring[19,20] combine to give peculiar field distributions along a hysteresis cycle, different than those expected for an infinitely long cylinder in Bean's critical state model.[17] The flux penetration and magnetization curves[21] as well as the ac susceptibility[22] of very thin rings have been theoretically studied by Brandt. He proposed an approximate analytical expression for the full penetration field in Bean's approximation. In addition, the magnetic behavior of thin-film rings has been experimentally studied by dc magnetometry,[23] ac susceptibility,[24,25] and magneto-optical imaging.[26] The case of melt-textured rings with intermediate finite dimensions, typically in the order of $R_i \sim 1.5$ mm internal, $R_0 \sim 2.45$ mm external radii and $L=0.1-2$ mm thickness, has not been systematically described yet.

In this paper we present a study of the irreversible magnetic behavior and the corresponding determination of the critical current density of melt-textured YBCO finite rings in the presence of perpendicular applied fields. The paper is structured as follows. In Sec. II we describe the experimental Hall probe imaging system employed for the ring magnetic characterization, and the numerical model used to calculate the finite superconducting ring's main magnetic characteristics. Section III A shows the influence of the ring's finite size on the magnetic field profiles. In Sec. III B we present expressions for the determination of the critical current density $J_c(H)$ dependence of finite rings, from either the integral magnetization loop $M(H)$ or the magnetic field induction cycle $B_c/\mu_0(H)$ at the center of the ring, measured by Hall imaging magnetometry. Section III C deals with the estimation of the critical current density from the full penetration field for finite rings, under the J_c constant approximation. In Sec. III D we will show how the $J_c(H)$ dependence influences the magnetization $M(H)$ curves of finite rings and describe the correct methodology that allows the J_c determination for arbitrary ring sizes. The conclusions are presented in the last section.

TABLE I. Dimensions of the rings investigated. Internal radius R_i, external radius R_0, thickness L, and aspect ratio figures $\delta = R_i/R_0$ and $\gamma = L/R_0$.

Sample	R_i (mm)	R_0 (mm)	L (mm)	$\delta = R_i/R_0$	$\gamma = L/R_0$
R017	1.63	2.45	0.17	0.67	0.07
R028	1.63	2.45	0.28	0.67	0.11
R053	1.63	2.45	0.53	0.67	0.22
R065	1.63	2.45	0.65	0.67	0.27
R07	1.63	2.45	0.70	0.67	0.29
R08	1.63	2.45	0.80	0.67	0.37
R125 (polished)	1.60	2.50	1.25	0.64	0.50
			1.10	0.64	0.44
			0.89	0.64	0.36
			0.60	0.64	0.24
R063	1.02	2.42	0.63	0.42	0.26

II. EXPERIMENT AND MODELING

Melt-textured $YBa_2Cu_3O_7$ rings were obtained from cylindrical pellets grown by the top-seeding method, following processes previously described.[14,27,28] The starting composition of the samples was either (i) a 75:25 mixture of Y123:Y211 powders with a 0.2 wt. % of PtO_2,[14,27] or (ii) 69 wt. % Y123+ 30 wt. % Y211+ 1 wt. % CeO_2.[28] Both methodologies gave high-J_c samples. Each pellet was sliced perpendicular to the c axis in disks of different thickness L ranging from 0.17 to 1.25 mm. Rings with an external diameter of ~5 mm and inner diameter ~3 mm were extracted from the disks by core drilling. Since the rings come from different pellets, the spread in J_c due to different material properties had to be taken into account. In order to minimize the effect of the J_c spread and focus only on the influence of the finite size of the ring, one of the rings (R125) was progressively thinned by polishing. Table I summarizes the dimensions of the rings analyzed. The normalized aspect ratio parameters $\delta = R_i/R_0$ and $\gamma = L/R_0$ have been introduced.

A Hall probe magnetic imaging system[29] was employed to obtain magnetic field induction distribution maps $B_z(x,y)$ of the rings at 77 K under magnetic fields in the range of 0–1 T, applied parallel to the c axis. This Hall imaging technique has been already widely tested in the characterization of other kind of superconducting samples, like YBCO cylinders,[30] YBCO/Ag/YBCO welds[31,32] or single-crystal YBCO foams.[33] The Hall probe used had an active area of 0.1×0.1 mm^2 and was rastered at a flying distance of $h \sim 80$ μm through the polished surface of the ring in steps of 160 μm. The system allows either recording the remanent $B_z(x,y,0)$ image after cooling the sample under an applied field (FC process), or the successive $B_z(x,y,H)$ images as the external magnetic field is increased, after zero-field-cooling the sample (ZFC process). In addition, the magnetic field induction cycle $B_c(H)$ at the central ring axis, at a distance ~80 μm from the ring surface was also recorded in just a few minutes time.

Additionally, the magnetic moment $m(H)$ of the rings was measured using a commercial superconducting quantum interference device (SQUID) magnetometer from Quantum Design (range 0–5.5 T, 5–300 K), a noncommercial low-field (range 0–200 G, 4–100 K) SQUID magnetometer or a vibrating sample magnetometer (VSM) from Lakeshore (range 0–7 T, 4–100 K).

On the other hand, a numerical method[34] was used to compute the characteristic curves describing finite rings.[35] The model basically solves the critical state in cylindrical coordinates assuming the ring to be composed of radial paths of current. The distribution of currents within the ring are obtained by minimizing the magnetic energy of the superconductor. Once this is known, the $B_z(x,y,H)$ profiles at a distance z above the ring and the $M(H)$ magnetization curves can be calculated. A solution can be obtained for both constant and field-dependent critical current density. This same theoretical approach was used to treat the critical state of finite cylinders.[34]

III. RESULTS AND DISCUSSION

A. Finite size effects on the rings field profiles

Within Bean's critical state model,[17] a ZFC infinitely long ring, under an increasing applied perpendicular magnetic field, would become fully penetrated by supercurrents at the field: $H_{\mathrm{pen}}^{\infty} = J_c(R_0 - R_i)$, where R_0 and R_i are, respectively, the external and internal radius of the ring. Field penetrates uniquely from the external radius of the ring, and the last penetrated point in the superconductor is at R_i. The center hole of the ring is completely magnetically shielded till $H_{\mathrm{pen}}^{\infty}$ is reached.

In finite rings, however, important demagnetization effects occur. Local fields H_r, owing to the shielding currents circulating in the ring, can close through the external surface of the ring but also via the central hole [Fig. 1(a)]. Hence, during initial flux penetration, a magnetic field $H_i = H - H_r$ is present inside the ring hole, even for applied magnetic fields smaller than $H_{\mathrm{pen}}^{\infty}$. As the applied field increases, flux penetration into the ring body progresses from two fronts simultaneously [Fig. 1(b)]: from R_0 to the ring body, due to the external field, and from R_i to the ring body radius, due to the field inside the hole. The last penetrated point in the superconductor and the full penetration field depend on the particular dimensions of the ring.

In order to study experimentally such finite size effects, we measured by Hall probe imaging the initial magnetic field distribution $B_z(x,y,H)$ profiles of ZFC rings with different aspect ratio, $\gamma = 0.5, 0.07, 0.27$ [Figs. 2(a)–2(c)]. Note that for all measured rings, a field inside the ring exists even below the field of full penetration, due to the flux lines of the local field H_r that close up via the central ring hole. These flux lines close up also via the external ring surface, resulting in a total field $H + H_r$ close to the wall larger than the applied field, as observed in the measured profiles [e.g., Fig. 2(b)]. These peculiar features have been also reported in thin-film rings studied by magneto-optical imaging.[26] The demagnetization effects become more important, and the profiles tend

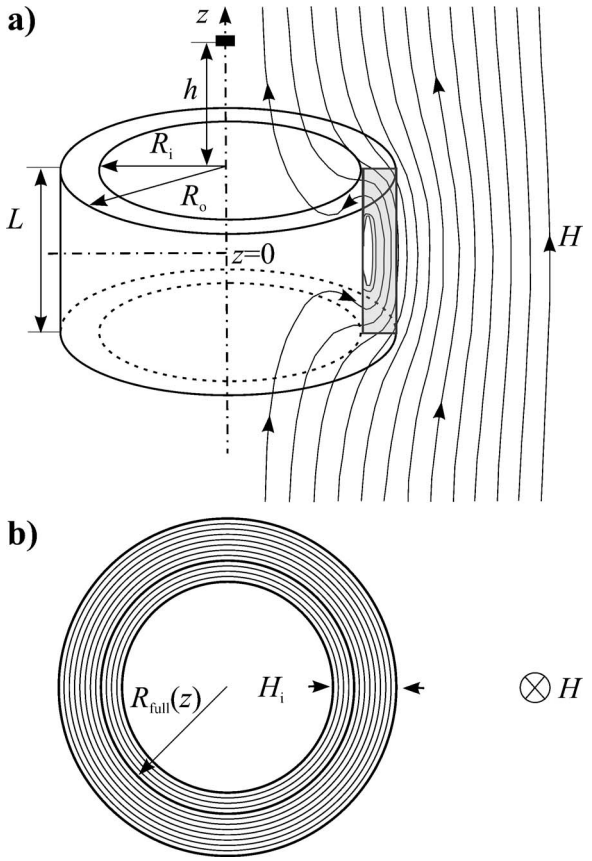

FIG. 1. (a) Typical dimensions and schematics of the field penetration in a ZFC finite ring. (b) Current circulation in a cross section at height z. In full penetration, the external and internal flux penetration fronts meet at $R_{\text{full}}(z)$.

to be sharper for thinner rings, as can be appreciated in Figs. 2(a)–2(c). For the thinnest ring measured (R017), the $B_z(x,H)$ profiles resemble the curves calculated by Brandt for thin-film rings.[18]

We have also reproduced theoretically the observed finite size effects, by computing the $B_z(x,H)$ field distributions with the help of a numerical program.[34,35] Figure 2(d) shows the calculated $B_z(x,H)$ profiles for the parameters of ring R017. The $J_c(H)$ dependence of the sample, which was obtained from the measured magnetic moment cycle $m(H)$, was entered as an input in the calculation. The profiles were calculated at different distances $h=z-L/2$ between ring surface and the Hall probe. Figure 2(d), left shows that the computed profiles become more rounded as h increases, as it may be expected. When the actual experimental gap of our setup ($h\sim 80$ μm) is considered, a good qualitative agreement between the computed [Fig. 2(d)] and the measured [Fig. 2(c)] curves is observed.

B. Hysteretic magnetization

The influence of the ring aspect ratio on the hysteretic magnetization cycles was studied by in-field Hall probe magnetometry. The local magnetization distribution maps as a function of the applied magnetic field were obtained by subtracting the applied magnetic field H from the measured

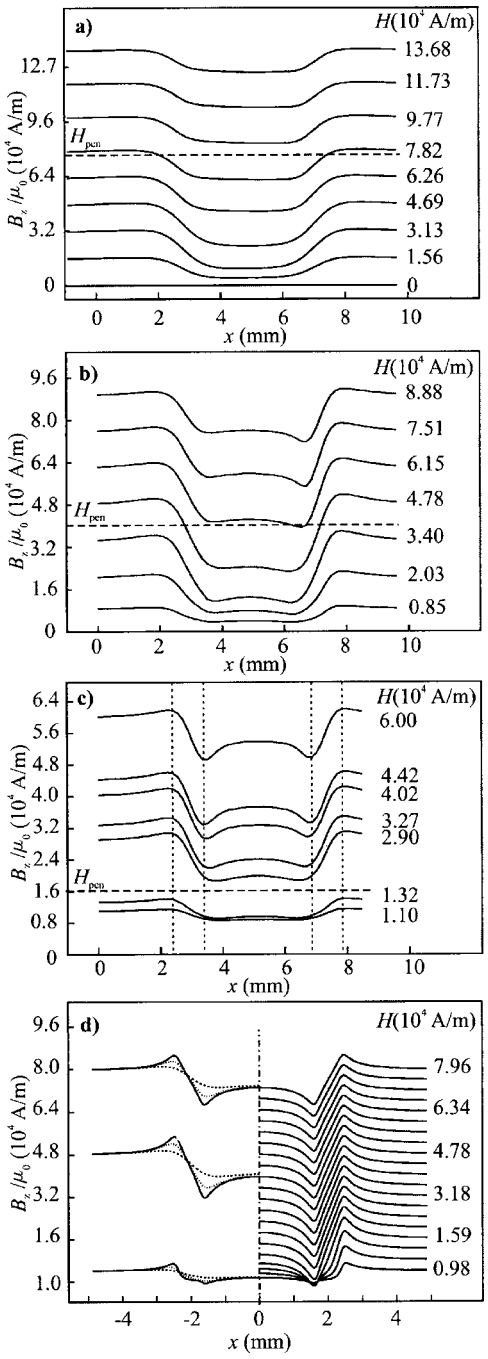

FIG. 2. Measured Hall probe $B_z/\mu_0(H)$ profiles along a diametral cross section for three rings with different aspect ratios: (a) R125 (γ=0.5), (b) R065 (γ=0.27), and (c) R017 (γ=0.07). (d) Calculated $B_z(H)$ profiles for ring R017. Right: at a height $h=80$ μm from the sample. Left: at different heights: $h=80$ μm (continuous line), $h=200$ μm (dotted line), and $h=500$ μm (dashed line).

$B_z(x,y,H)$ maps. By integration over the scanned area S, a hysteretic cycle $\langle B/\mu_0-H\rangle(H)$, directly proportional to the sample hysteretic magnetization $M(H)$, is obtained:

$$\langle B/\mu_0 - H\rangle(H) = \frac{1}{S}\int\int\left[\frac{Bz(x,y)}{\mu_0} - H\right]dxdy = \frac{M(H)}{k}. \quad (1)$$

Only a field-independent constant k, related to the geometry of the sample and the height of the scanning Hall probe is

needed to correlate the $\langle B/\mu_0 - H\rangle(H)$ cycle obtained by Hall magnetometry with the magnetization $M(H)=m(H)/V$ (where V is the ring superconducting volume) directly measured with a SQUID magnetometer.[29] The constant k can be determined theoretically as follows: a numerical method[34,35] is used to compute the current distribution in the sample, from which on one hand the sample magnetization M, and on the other the integrated magnitude $\langle B/\mu_0 - H\rangle$ at the Hall probe flying distance are calculated. k is then just the ratio $k=M/\langle B/\mu_0\rangle$. A good agreement ($\sim 5\%$) between the experimentally determined and calculated k constants was found for rings of different dimensions (R065, $k=113$; R017, $k=268$), thus demonstrating that Hall probe imaging could be used as an alternative to SQUID magnetometry for the determination of the magnetization cycles.

The critical current density dependence as a function of the applied field can then be obtained from the magnetization cycle $M(H)$ deduced from the integrated $\langle B/\mu_0 - H\rangle(H)$ measured by Hall probe imaging [Eq. (1)], using the analytical relation for finite rings developed in Ref. 35:

$$J_c(H) = \frac{3\Delta M(H)}{R_0}\left(1+\frac{\delta^2}{1+\delta}\right)^{-1}, \tag{2}$$

where $\Delta M(H)$ is the width of the magnetization loop in the saturated region.

On the other hand, thanks to the cylindrical symmetry of the problem, it is possible to extract $J_c(H)$ from the magnetic field induction measured at the center of the ring $B_c/\mu_0(H)$, instead of from the integrated $\langle B/\mu_0 - H\rangle(H)$ cycle. This possibility was applied, e.g., in Ref. 10, and discussed by Surzhenkho *et al.*[15] in the context of the determination of grain boundary critical currents in ring-shaped superconductors. It is easily deduced from Biot-Savart's law that the total field on the central axis created by a totally penetrated ring at a distance z from the central plane of the ring is[36]:

$$B_c = \frac{\mu_0}{2} J_c f(R_i, R_0, z);$$

$$f(R_i,R_0,z) = (L/2-z)\ln\left(\frac{R_0+\sqrt{R_0^2+(z-L/2)^2}}{R_i+\sqrt{R_i^2+(z-L/2)^2}}\right) + (L/2+z)\ln\left(\frac{R_0+\sqrt{R_0^2+(z+L/2)^2}}{R_i+\sqrt{R_i^2+(z+L/2)^2}}\right). \tag{3}$$

Therefore, the critical current field dependence is $J_c(H) = \Delta B_c/\mu_0 f(R_i,R_0,z)$, where $\Delta B_c = B_c^+ - B_c^-$ is the cycle width in the fully penetrated region. The advantage of this determination technique is that $B_c/\mu_0(H)$ can be simply and quickly measured with the help of just a Hall probe placed at the central ring axis at a distance h above the surface. Therefore, this setup could be easily installed in a cryogenic facility for the simple and fast acquirement of $J_c(H,T)$ curves.

The equivalence of the two $J_c(H)$ determination methods is exemplified for ring R125. The $\langle B/\mu_0 - H\rangle(H)$ and $B_c/\mu_0(H)$ cycles measured by Hall magnetometry are shown in Fig. 3(a). The $B_c/\mu_0(H)$ cycle is tilted with respect to the

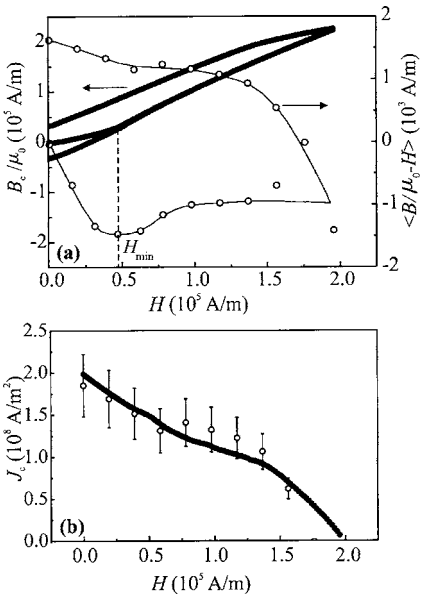

FIG. 3. (a) $B_c/\mu_0(H)$ cycle (●) measured with a Hall probe placed at the axis line of the ring, at $z=L/2+80$ μm, compared with the integral $\langle B/\mu_0 - H\rangle(H)$ (○) cycle (ring R125). (b) $J_c(H)$ dependences obtained from the $B_c/\mu_0(H)$ (●) and the $\langle B/\mu_0 - H\rangle(H)$ (○) cycles.

$\langle B/\mu_0 - H\rangle(H)$ cycle because the Hall probe at the ring center senses the sum of the field due to the induced currents and the applied field. Figure 3(b) shows the $J_c(H)$ dependences obtained from the $\langle B/\mu_0 - H\rangle(H)$ cycle and Eqs. (1) and (2) with a calculated factor $k \approx 145$ for this ring, and from the $B_c/\mu_0(H)$ cycle and Eq. (3), with $z=h+L/2\sim 1.33$ mm. A reasonable agreement is observed between the $J_c(H)$ curves determined by the two methods. It is also important to note that the magnetic field position of the "kink" in the initial curve H_{min} of both cycles coincides [Fig. 3(a)]. Therefore, the J_c determination based on the measurement of this point presented in the following sections will be possible by using indistinctly the integral $\langle B/\mu_0 - H\rangle(H)$ or the $B_c/\mu_0(H)$ cycles.

C. Penetration field in the Bean approximation

The full penetration field H_{pen} of a ring, defined as the minimum applied field at which a ZFC ring becomes fully penetrated by supercurrents, depends on the ring critical current density J_c and the ring dimensions, described by the parameters δ and γ. Therefore, if the relation between the full penetration field and sample dimensions is known, then the critical current density of the ring can be in principle obtained by simply measuring H_{pen} from the ring magnetization hysteretic cycle.

The magnetization curves of rings with different aspect ratio (δ,γ) were calculated using the numerical method,[34,35] assuming in a first approach a field-independent J_c. Figure 4(a) shows, for instance, the $M(H)$ curves for rings with $\delta=0.5$ and $\gamma=0.2,1,5$. The applied field and the magnetization have been normalized by the full penetration field of an infinitely long bulk cylinder, $H_{pen}^{\infty}=J_c R_0$, so that the cycles

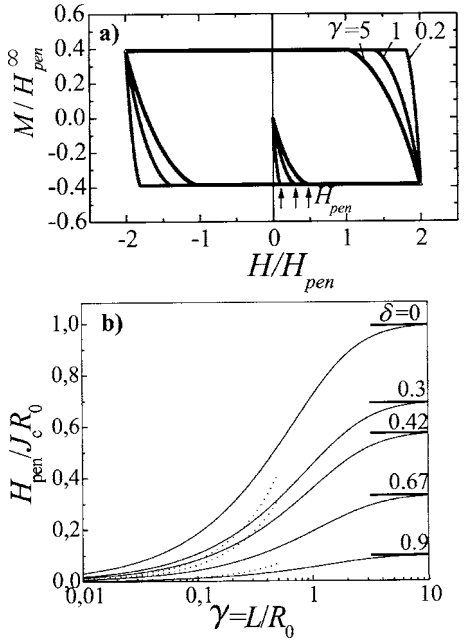

FIG. 4. (a) Magnetization loops for $\delta=0.5$ and different γ ratios: $\gamma=0.2,1,5$ in Bean's constant J_c approximation. The position of the fields of full penetration H_{pen} are indicated. (b) Theoretical normalized penetration field $H_{\mathrm{pen}}/J_c(0)R_0$ as a function of the aspect ratio γ: (continuous lines) analytical expression for finite rings [Eq. (4)], (dotted lines) Brandt's expression for very thin rings [Eq. (5)], and (thick lines) Bean infinite cylinder limit.

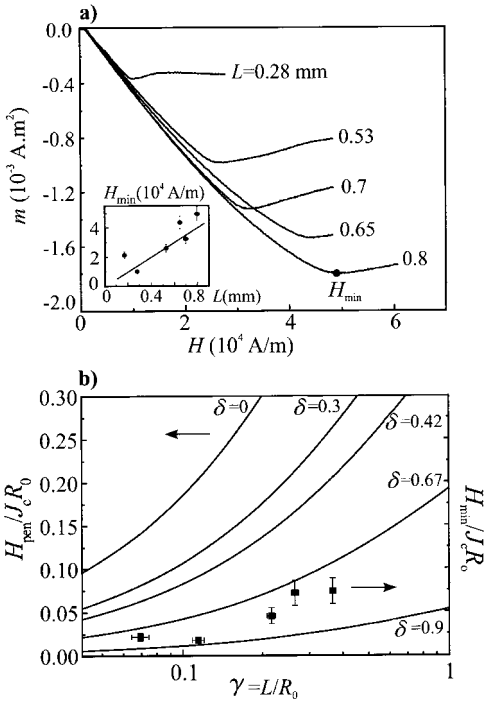

FIG. 5. (a) $m(H)$ cycles measured with SQUID magnetometry (thin lines) and Hall magnetometry (thick line) for the series of rings with equal internal $R_i/R_0=0.67$ and different thickness L. Inset: "kink" H_{min} vs ring thickness. (b) (■) Determined $H_{\mathrm{min}}/J_c(0)R_0$ values for this series of rings against the ($\delta=0.67$) analytical $H_{\mathrm{min}}/J_c(0)R_0$ curve.

are only dependent on adimensional parameters. It can be observed that the initial magnetization curve presents a "kink," which under the assumed J_c constant approximation, coincides exactly with the field of full penetration H_{pen}. For small γ ratios (thin rings), the slope of the initial magnetization curve becomes steeper, and H_{pen} is reached at smaller applied fields. For all cases, when $H>H_{\mathrm{pen}}$ the magnetization is the same, since the saturation magnetization is independent of γ in Beans's approach.

Based on the above numerical calculations, Navau *et al.* proposed an analytical expression for the full penetration field of arbitrary (δ,γ) finite rings:[35]

$$\frac{H_{\mathrm{pen}}}{J_cR_0}\approx\frac{\gamma}{2}\frac{(1-\delta)}{(1+\delta)}\ln\left\{\frac{2(1+\delta)}{\gamma}+\left[1+\left(\frac{2(1+\delta)}{\gamma}\right)^2\right]^{1/2}\right\}. \tag{4}$$

Figure 4(b) shows the normalized H_{pen}/J_cR_0 as a function of the aspect ratio γ for different δ values. The $\delta=0$ curve represents the particular case of a finite disk. Notice that Eq. (4) tends to Bean's limit $H_{\mathrm{pen}}^{\infty}/J_cR_0=1-\delta$ for an infinite cylinder $(\gamma\to\infty,x)$, and converges with the equation derived by Brandt[18] for very thin rings $(\gamma\ll1,\delta)$:

$$\frac{H_{\mathrm{pen}}}{J_cR_0}\approx\gamma\left[\frac{2}{\pi}\frac{(1-\delta)}{(1+\delta)}\left(\ln\frac{8(1+\delta)}{(1-\delta)}-1\right)-\frac{1}{2}(\ln\delta+1-\delta)\right]. \tag{5}$$

In order to study experimentally the dependence of the penetration field with the geometry and test the validity of Eq. (4), we measured the initial $m(H)$ curves of a series of rings with equal internal-to-external ratio ($\delta=R_i/R_0=0.67$) but different thicknesses [Fig. 5(a). The initial curve of each ring shows a "kink" at a field H_{min}, which increases with the ring thickness [see inset of Fig. 5(a)]. The scattering around this general behavior is due to spread in the material quality of the rings, which were extracted from different pellets. In previous papers, H_{min} was assimilated to the ring's full penetration field, and it was used to extract J_c.[14] We have now compared the experimentally determined $H_{\mathrm{min}}/J_c(0)R_0$ values for each ring, with the calculated (normalized) penetration field $H_{\mathrm{pen}}/J_c(0)R_0$ in Fig. 5(b). $J_c(0)$ was determined in each case from the complete $m(H)$ cycle measured by VSM (not shown) using Eq. (2). We find that the $H_{\mathrm{min}}/J_c(0)R_0$ values lie systematically below the analytical curve (between 15% and 60%), thus suggesting that the J_c values computed from H_{min} in finite sized rings are systematically too low. In the next section we will see that the field dependence of the critical current density is responsible for the deviation.

D. Influence of the $J_c(H)$ dependence

The effect of the $J_c(H)$ dependence[37] on the magnetization curves of finite rings of different ratio γ has been calculated using the numerical model described in Refs. 34 and 35. We assumed an exponential dependence of the form

$$J_c(H)=K\exp(-|H|/H_{\mathrm{oe}}),$$

where K and H_{oe} are positive constants. The parameter $p=KR_0/H_{\mathrm{oe}}$ is used to describe the strength of the exponential decay.

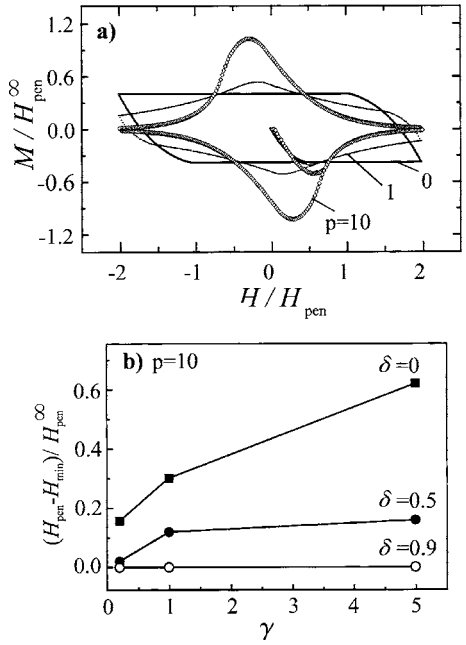

FIG. 6. (a) Magnetization loops for $\delta=0.5$, $\gamma=5$ and different $J_c(H)$ decays: $p=0,1,10$. (b) Difference between the full penetration field H_{pen} and the "kink" field H_{min} normalized by H^{∞}_{pen} as a function of γ, for $p=10$ and $\delta=0$ (disk), $\delta=0.5$, $\delta=0.9$.

Figure 6(a) shows the simulated magnetization loops for a given ring geometry ($\delta=0.5$, $\gamma=5$) and different $J_c(H)$ decays ($p=0$ corresponding to Bean's independent J_c model, $p=1$, and $p=10$). The curves are normalized to the penetration field of an infinite ring H^{∞}_{pen}. We can observe that for Bean's limit ($p=0$) the magnetization is flat for fields above the full penetration field H_{pen}, which is, by definition, the intersection between the initial and the return curves. Hence, in this case, $H_{pen}\equiv H_{min}$. However, as the p parameter becomes larger ($p>0$), the magnetization presents a "kink" in the initial curve at a field H_{min} smaller than the full penetration field, at the intersection point H_{pen}. The reason for this behavior is the following.

As the applied field is increased from zero, supercurrents penetrate further and further into the ring (both from the internal and external fronts, as argued in Sec. III A; but at the same time, the values of these currents become progressively smaller, due to the critical current dependence on the internal field. This results in two competing trends: as a larger volume of ring is penetrated, the (absolute) magnetization tends to increase, whereas as J_c decreases, M tends to decrease. The minimum in the initial magnetization curve at H_{min} occurs when the later tendency starts prevailing over the first one. Note that at this point, the ring is not necessarily fully penetrated by currents, a situation that is only accomplished at a higher field H_{pen}.

Our simulations show that for a given $J_c(H)$ dependence (parameter p), the (normalized) difference between H_{pen} and H_{min} becomes larger for increasingly thick (large γ) and broad (small δ) rings [Fig. 6(b)], whereas for sufficiently thin ($\gamma<0.2$), narrow ($\delta>0.5$) rings, H_{pen} and H_{min} practically coincide regardless of the $J_c(H)$ dependence.

We have experimentally observed the difference between H_{pen} and H_{min} in the magnetization curves of thick rings. For

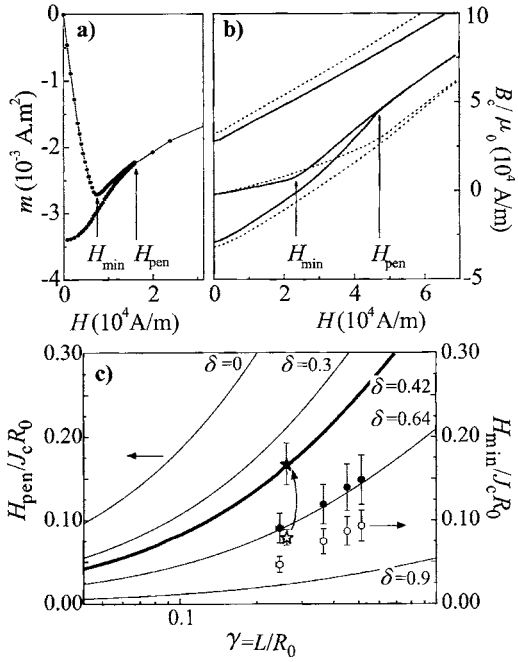

FIG. 7. (a) $m(H)$ cycle of ring R063. (b) $B_c(H)$ cycles for ring R125 with thickness $L=1.25$ mm (continuous line), and same ring polished into thickness $L=0.6$ mm (dashed line). H_{min} and H_{pen} are indicated. (c) Ring R063: Theoretical $H_{pen}/J_c(0)R_0$ (thick line, $\delta=0.42$) and experimentally determined $H_{min}/J_c(0)R_0$ (star) and $H_{pen}/J_c(0)R_0$ (bold star). Series of polished rings R125: Theoretical $H_{pen}/J_c(0)R_0$ ($\delta=0.64$) and experimentally determined $H_{min}/J_c(0)R_0$ (○) and $H_{pen}/J_c(0)R_0$ (●).

instance, Fig. 7(a) shows the $m(H)$ curve of ring R063 ($\delta=0.42$, $\gamma=0.26$, $p\approx 1.2$). We studied as well the influence of the ring thickness on the $B_c/\mu_0(H)$ cycles, which, as justified in Sec. III B, can be used alternatively to the integral magnetization cycle to determine the J_c. A thick ring R125 was successively polished and $B_c/\mu_0(H)$ measured. Figure 7(b) shows, e.g., the cycles measured for two of the ring thicknesses (the others are omitted for the sake of clarity), where the difference between the position of the "kink" at H_{min} in the initial $B_c(H)$ curve and the full penetration point H_{pen} can be clearly seen.

From these two values, we determined the normalized $H_{min}/J_c(0)R_0$ and $H_{pen}/J_c(0)R_0$ for each ring thickness, γ, and plotted them against the analytical value given by Eq. (4). The $J_c(0)$ values needed for the normalization were calculated either from the complete $m(H)$ cycle and Eq. (2), or $B_c/\mu_0(H)$ and Eq. (3). Figure 7(c) summarizes the results. For ring R063, we can observe that while $H_{min}/J_c(0)R_0$ lies $\sim$50% beneath the theoretical curve ($\delta=0.42$), the experimental value $H_{pen}/J_c(0)R_0$ value coincides with it. For the series of polished rings (R125), the $H_{min}/J_c(0)R_0$ values fall systematically below the curve, whereas the $H_{pen}/J_c(0)R_0$ values are well described by the analytical Eq. (4) of $\delta=0.64$. Note also that as the ring becomes thinner, the $H_{min}/J_c(0)R_0$ value approaches $H_{pen}/J_c(0)R_0$, as predicted by the presented simulations.

From the above results it can be concluded that for real YBCO superconducting thick rings, the $J_c(H)$ dependence

introduces a shift of H_{pen} with respect to H_{min}, and therefore it is not strictly correct to use the "kink" value of the magnetization [or $B_c/\mu_0(H)$] for the calculation of J_c. At most, this method can be just used to get a rough, quick estimation of J_c, bearing in mind that the value will be underestimated (by about 40% for a thick ring with $\gamma \sim 0.5$). Instead, the correct determination of the critical current based on the measurement of the full penetration field should be done considering the intersection point between the initial and return curves measured from the complete magnetization cycle. Only for sufficiently thin ($\gamma < 0.2$), narrow ($\delta > 0.5$) rings, $H_{min} \approx H_{pen}$, and the "kink" of the initial curve will give a good estimation of J_c.

Hence, the methodological recommendation for the simple determination of the critical current density in superconducting YBCO rings could be summarized as follows: Thin rings with large inner holes (narrow rings) should be selected. Then, measure the initial $B_c/\mu_0(H)$ curve with a Hall probe centred on top of the ring, and introduce the value of the field H_{min}, which can be very accurately determined from the second derivative $\partial^2 B_c/\partial H^2(H)$, in Eq. (4) to obtain $J_c(0)$. Using this methodology on a thin ring (R017, $\gamma = 0.07$), we obtained[35] a very good agreement (within 2%) between the experimentally and calculated values of $J_c \approx 4.01 \times 10^8$ A/m^2.

IV. CONCLUSIONS

The magnetic behavior of melt-textured $YBa_2Cu_3O_7$ finite rings in perpendicular magnetic fields has been investigated using an in-field Hall probe magnetic imaging system. This system allows the analysis of the evolution of the distribution of the magnetic field induction when the external magnetic field is cycled, as well as the measurement of the integral $M(H)$ cycle upon integration of the local magnetic field. By recording the ring $B_z(x,y,H)$ maps for increasing fields we have shown that, due to the demagnetizing effects, a magnetic field exists inside the ring hole, and thus flux penetration progresses both from the outer and inner radius fronts into the ring body. The effect of the ring size on the hysteretic magnetization curves has been studied both experimentally and by numerical calculation of the $M(H)$ curves of rings with different aspect ratios. An analytical expression for the determination of the critical current density of finite rings based on the measurement of the full penetration field was presented and experimentally tested. We showed that due to the dependence of the critical current density with the internal magnetic field, the magnetization initial curve shows a "kink" at an applied magnetic field H_{min}, which is in general different from the field of full penetration H_{pen}. The correct determination of J_c should be done using this later magnetic field. Only for very thin/narrow rings, the two fields approximately coincide $H_{min} \approx H_{pen}$, and hence the "kink," can be used to determine the critical current density. Since the "kink" can be very simply and accurately determined from the initial $B_c/\mu_0(H)$ curve measured just at the center of the ring, this methodology opens the door for a fast and simple determination of $J_c(T,H)$ curves.

ACKNOWLEDGMENTS

This work was supported by the Spanish Science Ministry (MAT2003-01584), by the Generalitat de Catalunya (Catalan Pla de Recerca 00206 and CeRMAE) and the European project SUPERMACHINES (RTN1-1999-00282). E.B. wishes to thank the CSIC (Consejo Superior de Investigaciones Científicas, Spain) for financial support.

[1] T. Suzuki, H. Suzuki, M. Endo, Y. Yasaka, H. Marimoto, H. Takaichi, and M. Murakami, Adv. Supercond., 1983 **6**, 1237 (1994); H. Teshima, S. Sukuka, and R. Shimada, *ibid.* **12**, 806 (2000).

[2] H. Teshima, S. Sukuka, and R. Shimada, Adv. Supercond., 1983 **12**, 806 (2000).

[3] S. R. Curras, R. Santos, G. Domarco, A. Déaz, J. A. Veira, J. Maza, M. X. Francois, and F. Vidal, Cryogenics **37**, 653 (1997).

[4] M. Chen, T. Baumann, P. Unternahrer, and W. Paul, Physica C **282**, 2639 (1997).

[5] H. Zhen, M. Jiang, R. Nikolova, V. Vlasko-Vlasov, Y. Welp, B. W. Veal, G. W. Crabtree, and H. Claus, Physica C **309**, 17 (1998).

[6] M. R. Osorio, L. Cabo, J. A. Veira, and F. Vidal, Supercond. Sci. Technol. **17**, 98 (2004).

[7] K. Kanbara, T. Takizawa, H. Matsuura, and R. Shimadate, Physica C **156**, 727 (1988).

[8] R. Gross, P. Chaudhari, A. Gupta, and G. Koreu, Physica C **166**, 277 (1990).

[9] C. E. Gough, A. Gencer, G. Yang, M. Z. Shoustari, A. I. M. Rae, and J. S. Abell, Cryogenics **33**, 339 (1993).

[10] H. Darhmaoui and J. Jung, Phys. Rev. B **53**, 14621 (1996).

[11] W. Paul and Th. Baumann, Physica C **175**, 102 (1999).

[12] J. Jung, I. Isaac, and M. A-K. Mohamed, Cryogenics **32**, 988 (1992).

[13] K. Salama and V. Selvamanickan, Appl. Phys. Lett. **60**, 898 (1992); W. Lo, D. A. Cardwell, A. D. Bradley, R. A. Doyle, Y. H. Shi, and S. Lloyd, IEEE Trans. Appl. Supercond. **9**, 2042 (1999); L. Chen, H. Claus, A. P. Paulikas, H. Zheng, and B. W. Veal, Supercond. Sci. Technol. **15**, 1 (2002); S. Iliescu, X. Granados, E. Bartolomé, S. Sena, A. E. Carrillo, T. Puig, X. Obradors, and J. E. Evetts, *ibid.* **16**, 1 (2003).

[14] H. Claus, U. Welp, H. Zheng, L. Chen, A. P. Paulikas, B. W. Veal, K. E. Gray, and G. W. Crabtree, Phys. Rev. B **64**, 144507 (2001).

[15] A. B. Surzhenkho, M. Zeisberger, T. Habisreuther, W. Gawalek, and L. S. Uspenskaya, Phys. Rev. B **68**, 064504 (2003).

[16] J. R. Thompson, H. J. Kim, C. Cantoni, D. K. Christen, R. Feenstra, and D. T. Verebelyi, Phys. Rev. B **69**, 104509 (2004).

[17] C. P. Bean, Phys. Rev. Lett. **8**, 250 (1962); C. P. Bean, Rev. Mod. Phys. **36**, 31 (1964).

[18] E. H. Brandt, Phys. Rev. B **55**, 14513 (1997).

[19] S. Senoussi, S. Hadjoudj, R. Maury, and A. Fert, Physica C **165**, 364 (1990).

[20] K. L. Telschow and L. S. Koo, Phys. Rev. B **50**, 6923 (1994).
[21] E. H. Brandt, Phys. Rev. B **58**, 6506 (1998); E. H. Brandt, *Physics and Materials Science of Vortex States, Flux Pinning and Dynamics*, edited by R. Kossowsky *et al.* (Kluwer Academic, The Netherlands, 1999), p. 81.
[22] E. H. Brandt, Phys. Rev. B **55**, 14513 (1997).
[23] E. S. Borovitskaya, V. M. Genkin, and G. I. Leviev, IEEE Trans. Appl. Supercond. **7**, 1220 (1997).
[24] Th. Herzog, H. A. Radovan, P. Ziemann, and E. H. Brandt, Phys. Rev. B **56**, 2871 (1997).
[25] F. Mrowka, M. Wurlitzer, P. Esquinazi, E. H. Brandt, M. Lorenz, and K. Zimer, Appl. Phys. Lett. **70**, 898 (1997).
[26] M. Pannetier, F. C. Klaassen, R. J. Wijngaarden, M. Welling, K. Heeck, J. M. Huijbregtse, B. Dam, and R. Griessen, Phys. Rev. B **64**, 144505 (2001).
[27] H. Zheng, H. Claus, L. Chen, A. P. Paulikas, B. W. Veal, B. Olsson, A. Koshelev, J. Hull, G. W. Crabtree, and G. A. Boyd, Physica C **350**, 17 (2001).
[28] X. Obradors, R. Yu, F. Sandiumenge, B. Martinez, N. Vilalta, V. Gomis, T. Puig, and S. Piñol, Supercond. Sci. Technol. **10**, 884 (1997).
[29] X. Granados, S. Sena, E. Bartolomé, A. Palau, T. Puig, X. Obradors, M. Carrera, J. Amorós, and H. Claus, IEEE Trans. Appl. Supercond. **13**, 3667 (2003).
[30] M. Carrera, J. Amorós, X. Obradors, and J. Fontcuberta, Supercond. Sci. Technol. **16**, 1187 (2003).
[31] S. Iliescu, S. Sena, X. Granados, E. Bartolomé, T. Puig, X. Obradors, M. Carrera, J. Amorós, S. Krakunovska, and T. Habisreuther, IEEE Trans. Appl. Supercond. **13**, 3136 (2003).
[32] S. Iliescu, S. Sena, X. Granados, E. Bartolomé, T. Puig, X. Obradors, M. Carrera, J. Amorós, S. Krakunovska, and T. Habisreuther, IEEE Trans. Appl. Supercond. **13**, 3136 (2003).
[33] E. Bartolomé, X. Granados, T. Puig, X. Obradors, E. S. Reddy, and G. J. Schmitz, Phys. Rev. B **70**, 144514 (2004).
[34] A. Sanchez and C. Navau, Phys. Rev. B **64**, 214506 (2001).
[35] C. Navau, A. Sánchez, E. Pardo, E. Bartolomé, X. Granados, T. Puig, and X. Obradors Phys. Rev. B **71**, 214507 (2005).
[36] J. D. Jackson, *Classical Electrodynamics* (Wiley, New York, 1962).
[37] B. Martínez, T. Puig, A. Gou, V. Gomis, S. Piñol, J. Fontcuberta, X. Obradors, and G. Chouteau, Phys. Rev. B **58**, 15198 (1998).